Conformational Equilibria of Multimodal

Chromatography Ligands in Water and Bound to

Protein Surfaces

Camille L. Bilodeau[†](bilodc2@rpi.edu), Edmond Y. Lau[‡](lau12@llnl.gov), Steven M.

Cramer[†](crames@rpi.edu), Shekhar Garde[†]*(gardes@rpi.edu)

[†]Howard P. Isermann Department of Chemical and Biological Engineering and Center for Biotechnology and Interdisciplinary Studies, Rensselaer Polytechnic Institute, 110 Eighth Street, Troy, New York 12180, United States

[‡]Physical and Life Sciences Directorate, Lawrence Livermore National Laboratory, Livermore,
California, 94550, United States of America

Abstract:

Multimodal chromatography uses small ligands with multiple modes of interaction, e.g., charged, hydrophobic, or hydrogen bonding, to separate proteins from complex mixtures. The mechanism by which multimodal ligands interact with proteins is expected to be affected by ligand conformations, among other factors. Here, we study conformational equilibria of two commercially used multimodal cation exchange ligands, Capto MMC and Nuvia cPrime, in a range of solvents – a Lennard Jones (LJ) liquid, ethanol, and water – using molecular dynamics (MD)

simulations. By mapping ligand conformations onto two key torsion angles, ω and φ , in these solvents and in low and high dielectric media, we quantify the relative importance of intramolecular and solvent-mediated interactions. In a high dielectric medium Capto MMC preferentially samples three conformations, which are stabilized by a combination of an intramolecular torsion potential (on ω) and LJ interactions. In an LJ liquid, solvent molecules compete with intramolecular interactions while simultaneously providing an osmotic force, stabilizing both closer and farther distances between ligand sites. This has the overall effect of 'flattening out' the conformational landscape. Interestingly, in ethanol and water, hydrogenbonding between the amide hydrogen and solvent molecules stabilizes two additional conformations of Capto MMC in which ω takes on less favorable cis-like configurations. MD simulations of ligands in free solution with three therapeutic antibody fragments show that ligand conformational equilibria remain effectively unchanged upon binding to proteins. Although, there is 20-30% dehydration of the overall ligand upon binding, the hydrogen-bonding sites are dehydrated to a much smaller extent, particularly in cis-like configurations. Conformational preferences of Nuvia cPrime are similar to that of Capto MMC, except for the effect of symmetry arising from the absence of an alkyl thiol tail. Characterizing the conformational equilibria of these two ligands in free solution and bound to a protein provides a foundation for developing a mechanistic understanding of protein-multimodal ligand interactions.

1. Introduction

Many important biomolecular phenomena occur in an aqueous medium¹⁻³. The packing and orientations of water molecules in the vicinity of a solute depend on the solute chemistry and architecture. This water structure, in turn, influences the conformational equilibria of flexible solutes and their interactions with other molecules. The connection between water structure and

water-mediated interactions has been explored in numerous systems ranging from simple ones (e.g., hydrophobic interactions between methane molecules or conformational equilibria of lower alkanes in water)^{4–6} to complex ones (e.g., conformational equilibria and interactions of peptides and proteins in water)^{7–9}.

For example, short alkanes adopt linear conformations in water, while longer and more flexible chains collapse into compact, globular states driven by water-mediated interactions^{10–13}. These globular states transform into hairpin structures when a pair of charged groups is included in an otherwise hydrophobic polymer sequence¹⁴. Similar studies of the alanine dipeptide and other small, model peptides using methods ranging from classical and *ab initio* simulations to experiments have highlighted the role of water in governing conformational equilibria^{9,15–20}. Environmental effects, such as the introduction of an air-water interface, can significantly perturb water structure, and therefore can dramatically affect water-mediated interactions and conformational equilibria of molecules^{21–23}.

Here, we are interested in studying the conformational equilibria of flexible, multimodal solutes that are employed in a class of chromatography used for protein separations, called multimodal chromatography. In contrast to single mode chromatography (*e.g.*, hydrophobic or ion-exchange), multimodal chromatography uses ligands containing multiple modes of interaction including charge, aromatic, hydrophobic, and hydrogen bonding to separate proteins. Manipulation of the protein-ligand interactions by changing solution conditions provides a handle on separation. This strategy has been found to be more effective than other methods at purifying difficult-to-separate proteins^{24–29}. Despite these advantages, the complexity of protein-multimodal ligand interactions makes overall chromatographic behavior difficult to understand and predict^{30,31}. The lack of

fundamental understanding of these systems poses a significant barrier to multimodal process development and ligand design.

As an important step toward fundamentally understanding interactions in multimodal chromatography, here we use molecular dynamics simulations to study the hydration and conformational equilibria of two commonly used, commercially available ligands, Capto MMC and Nuvia cPrime, in water and in the vicinity of proteins. Specifically, we address the following questions: what are the conformational equilibria of these ligands in water? What role do intramolecular and water-mediated interactions play in governing conformational preferences? How do conformations change when the ligand binds to proteins? By studying the behavior of ligands in vacuum and in different granular solvents, we evaluate the relative importance of intramolecular and solvent-mediated interactions in determining ligand conformations. Specifically, simulations of ligands in a Lennard-Jones (LJ) liquid, ethanol, and water allow us to distinguish between the role of the attractive field of a granular solvent (e.g., an LJ liquid) and the increasingly directional hydrogen-bonding interactions present in ethanol and water. Finally, studying ligand conformations in the vicinity of fragments of therapeutic antibodies sheds light on the role of protein-ligand-water interactions in these complex systems.

2. Methods

Capto MMC (GE Healthcare, Chicago, IL) and Nuvia cPrime (Bio-Rad Laboratories, Hercules, CA) are two commercially available chromatography ligands that are commonly used in protein separations³² and have a shared structural motif. Both ligands contain four chemical groups – a negatively charged group (carboxylic acid) and a hydrophobic group (phenyl ring), connected by a hydrophilic peptide bond (Figure 1a). The fourth group differs between the two ligands: Capto

MMC contains an alkyl thiol group on one end, while Nuvia cPrime contains an amine group at the para position of the phenyl ring. In a typical application, these ligands are covalently linked to the base matrix of a chromatographic resin. Capto MMC is immobilized to a bead having an agarose base matrix via an ester linker attached to the end of the alkyl thiol group of Capto MMC. Nuvia cPrime, in contrast, is directly immobilized to a bead with a polyacrylamide base matrix via the amine group³³.

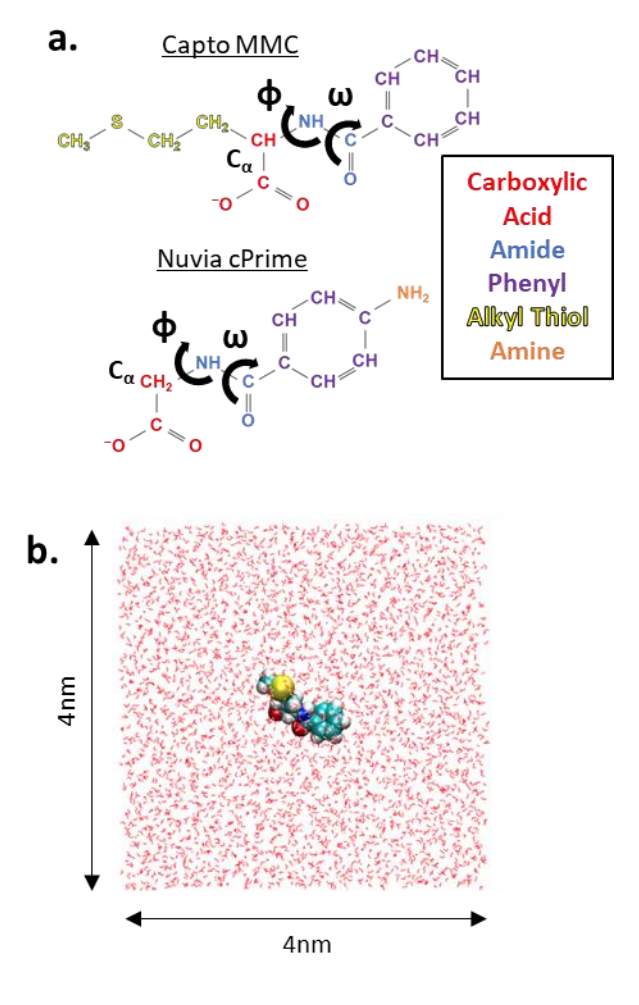


Figure 1. (a) Chemical structures for multimodal ligands Capto MMC and Nuvia cPrime. Color indicates the type of chemical moiety. Torsion angle ω corresponds to the O-C-N-H angle within the amide group and torsion angle ω refers to the C-N-C-C angle between the amide and carboxylic acid groups. C α refers to the carbon at the base of the carboxylic acid group. (b) A snapshot from MD simulations of the Capto MMC ligand (spacefill) in water (wireframe).

The 3D periodic box has dimensions of ~4nm x 4nm. Color scheme: hydrogen, white; oxygen, red; carbon, cyan; nitrogen, blue; and sulfur, yellow.

As an important step toward understanding key interactions in multimodal chromatography, we quantify conformational preferences of the two ligands in water and near proteins. The conformational equilibria of ligands can be characterized in many ways, for example, using a distribution of the end-to-end distance or other internal coordinates. Here, we calculate the probability distributions of two important torsion angles, ω and φ , which are located near the center of each ligand (Figure 1a). ω refers to the O-C-N-H torsion angle within the amide bond, where ω = 0° corresponds to those four atoms in the cis conformation. φ refers to the C-N-C-C torsion angle, where φ = 0° corresponds to those four atoms in the cis conformation.

The conformational equilibria of Capto MMC and Nuvia cPrime are governed by a combination of intramolecular and solvent-mediated interactions. To understand and quantify these contributions, we performed simulations of these ligands (i) in vacuum, (ii) in various solvents ranging from a continuum dielectric to explicit water, and (iii) in aqueous solutions with proteins (shown in Figure 1b). In all of these simulations, ligand force-field parameters were obtained from the General AMBER Force Field (GAFF)³⁴ while for atomic partial charges were obtained using a GAUSSIAN calculation with RESP assignment using the Antechamber tool of AMBER^{35–38} (See SI for charge assignments). All molecular dynamics simulations were performed using GROMACS 4.5.3.

2.1 Simulations of ligands in vacuum

The conformational equilibria of a ligand in vacuum are governed solely by intramolecular interactions, which include bonded interactions (i.e., bond-length, angle, and torsion) and non-bonded interactions (i.e., LJ and electrostatic interactions). To understand how bonded and non-

bonded interactions affect conformational preferences, we performed simulations of each ligand in vacuum with (i) only bonded interactions (without LJ or electrostatics), (ii) bonded and LJ interactions, and (iii) all intramolecular interactions including electrostatic interactions. We also simulated each ligand in a dielectric medium with dielectric constant, $\varepsilon = 78$, to understand the effect of screening charge interactions on ligand conformation.

Simulations of a single ligand placed at the center of a cubic box of 4nm length were performed in the NVT ensemble with Replica Exchange Molecular Dynamics (REMD) method to enable conformational sampling^{39–41}. Temperatures were chosen based on an exponential distribution using the web server developed by Patriksson et al.⁴² and adjusted to achieve an exchange rate of ~0.25. Five replicas were simulated for each system and with T = 298K, 390, 510K, 670K, and 860K, maintained using the Nosé-Hoover thermostat⁴³. Three central ligand atoms were restrained in each simulation with a harmonic potential of 1,000 kJ/mol/nm² to prevent 'the flying ice cube' problem⁴⁴. Simulations were run for 10ns, storing coordinates every 1ps. Electrostatics were calculated using the Generalized Reaction Field method⁴⁵ and periodic boundary conditions were turned off.

2.2 Simulations of ligands in solution

We studied conformational equilibria of ligands in three different solvents: a Lennard-Jones liquid, ethanol, and water. A single ligand molecule was placed at the center of the box and was solvated by sufficient number of solvent molecules (for Capto MMC: $N_{LJ} = 1400$, $N_{Ethanol} = 699$, $N_{water} = 2213$; for Nuvia cPrime: $N_{LJ} = 1400$, $N_{Ethanol} = 700$, $N_{water} = 2216$) to fill a cubic box of ~4nm length. Simulations were performed^{39–41} in the NPT ensemble, where temperature (298K) and pressure (1 bar) were maintained using Nose-Hoover thermostat⁴³ and Parinello-Rahman

barostat⁴⁶, respectively. Electrostatic interactions were calculated using the Particle-Mesh Ewald method⁴⁷.

Interaction parameters for the LJ liquid were chosen to obtain a thermodynamic state point in the liquid phase (T*= 1.11, ρ *= 0.86). Ethanol was represented using GAFF (where partial atomic charges were obtained using a GAUSSIAN calculation with RESP assignment performed using Antechamber module of AMBER)^{34–38,48} and a TIP4P model was used to represent water molecules^{49,50}. We also performed simulations of ligands in TIP3P water – conformational equilibria in those simulations are similar to that in TIP4P water (see SI). Analyses were performed from a 10ns long trajectory using coordinates stored every 1ps.

2.3 Ligands in the Presence of Proteins

To characterize ligand conformational equilibria in the vicinity of proteins, we performed simulations of ligands in aqueous solution of proteins. We studied three therapeutic proteins of interest that were fab fragments of an antibody, referred to here as Fab A, Fab B, and Fab C⁵¹. Each simulation included 64 copies of a ligand (~0.1M concentration), one protein molecule, and sufficient number of water molecules (~29,500, exact numbers can be found in SI) to fill a box of size 9.5nm x 10nm x 12nm, allowing for a margin of ~1.5nm on each side of the protein. Proteins were represented using the AMBER99 force-field⁵² and water using the TIP3P model. Simulations were performed^{39–41} in the NPT ensemble, where temperature (298K) and pressure (1bar) were maintained using the Nosé-Hoover thermostat⁴³ and the Parrinello-Rahman barostat⁴⁶. Equilibration runs of 50ns were followed by 150ns production runs, where frames were stored every 1ps. Four buried alpha carbons in the center of each fab domain were restrained using a harmonic potential with a constant of 40,000 kJ/mol/nm² to prevent translation and rotation of the protein.

3. Results and Discussion

Figure 2a and 2b show conformational equilibria of Capto MMC and Nuvia cPrime in water as quantified by the joint probability distribution, $p(\omega, \varphi)$, obtained from MD simulations. For Capto MMC, four distinct peaks (or clusters of conformations) emerge, labelled A through D in Figure 2a, representing preferentially sampled conformations in the φ - ω space. The intramolecular torsion potential on ω has a favorable minimum corresponding to the *trans* conformation (ω = 180°) and a less favorable minimum corresponding to the *cis* conformation (ω = 0° or 360°). Indeed, conformations A, B, and C, are centered on the ω = 180° line, while conformation D overcomes the torsion potential on ω , resulting in *cis*-like amide geometries. In contrast to ω , the GAFF force-field does not contain a torsion potential on φ . Thus, preference for discreet values of φ observed in Figure 2a must result from a combination of intramolecular interactions and solvent-mediated interactions.

Nuvia cPrime preferentially samples only three conformations, A, B, and D. Nuvia cPrime is similar in chemical structure to Capto MMC but lacks the alkyl thiol tail, resulting in a two-fold screw symmetry about the central carbon, referred to here as C_{α} (shown in Figure 2b). Therefore, A', B', and D' simply reflect the symmetric counterparts of A, B, and D. Conformations A and B are characterized by a planar *trans* ω , while conformation D is *cis*-like. These conformational preferences are consistent with existing crystal structures of Nuvia cPrime (also known as 4-amino hippuric acid), which contain torsion angles of -175.5° and 105.8° for ω and ϕ respectively. Again, preference for discreet values of ϕ for Nuvia cPrime conformations is similar to that for Capto MMC in water. We explore the role of intramolecular and solvent-mediated interactions below to help understand the conformational preferences observed here in water.

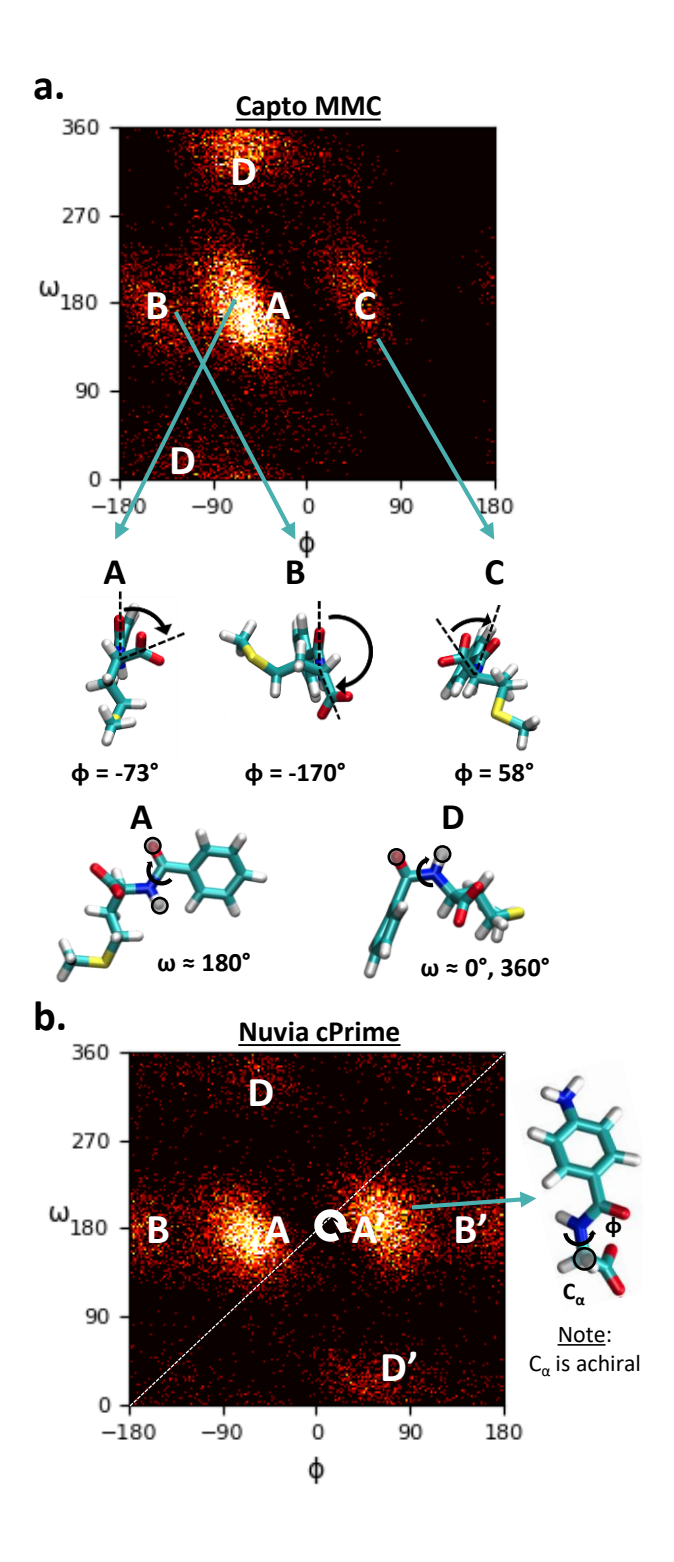


Figure 2. (a) Joint probability distribution for ϕ - ω torsion angles for Capto MMC in water. Probability is normalized such that the sum over the area is 1. Representative structures for conformations A, B, and C are shown for Capto MMC, highlighting their differences in torsion angle ϕ . Representative structures for conformations A and D are

shown for Capto MMC highlighting their differences in torsion angle ω . (b) Joint probability distribution for φ - ω torsion angles for Nuvia cPrime in water. Dotted line indicates the Nuvia cPrime symmetry plane resulting from the achiral C_{α} . Representative structure for Nuvia cPrime with C_{α} labelled is shown. All ligand structures are shown in licorice (hydrogen, white; oxygen, red; carbon, cyan; nitrogen, blue; sulfur, yellow).

3.1 The Intramolecular Contribution: Conformational Equilibria in Vacuum

As described in the methods section, the intramolecular contribution contains two components: bonded interactions and non-bonded interactions. We first simulate the molecules using only the bonded interactions to identify the inherent conformational preferences of the molecules unencumbered by excluded volume effects, electrostatics, or solvent contributions (Figure 3a). We then add LJ interactions (Figure 3b) followed by adding electrostatic interactions (Figure 3c).

Figures 3a and 3d show the conformational preferences of Capto MMC and Nuvia cPrime, respectively, governed solely by bonded interactions. Unsurprisingly, we find that both molecules prefer $\omega = 0^{\circ}$, 180° , and 360° , in keeping with their torsion potentials, while having no preference for any value of φ (which does not have a torsion potential acting on it). We note that for both ligands, as expected, these conformations favor $\omega = 180^{\circ}$ over $\omega = 0^{\circ}/360^{\circ}$.

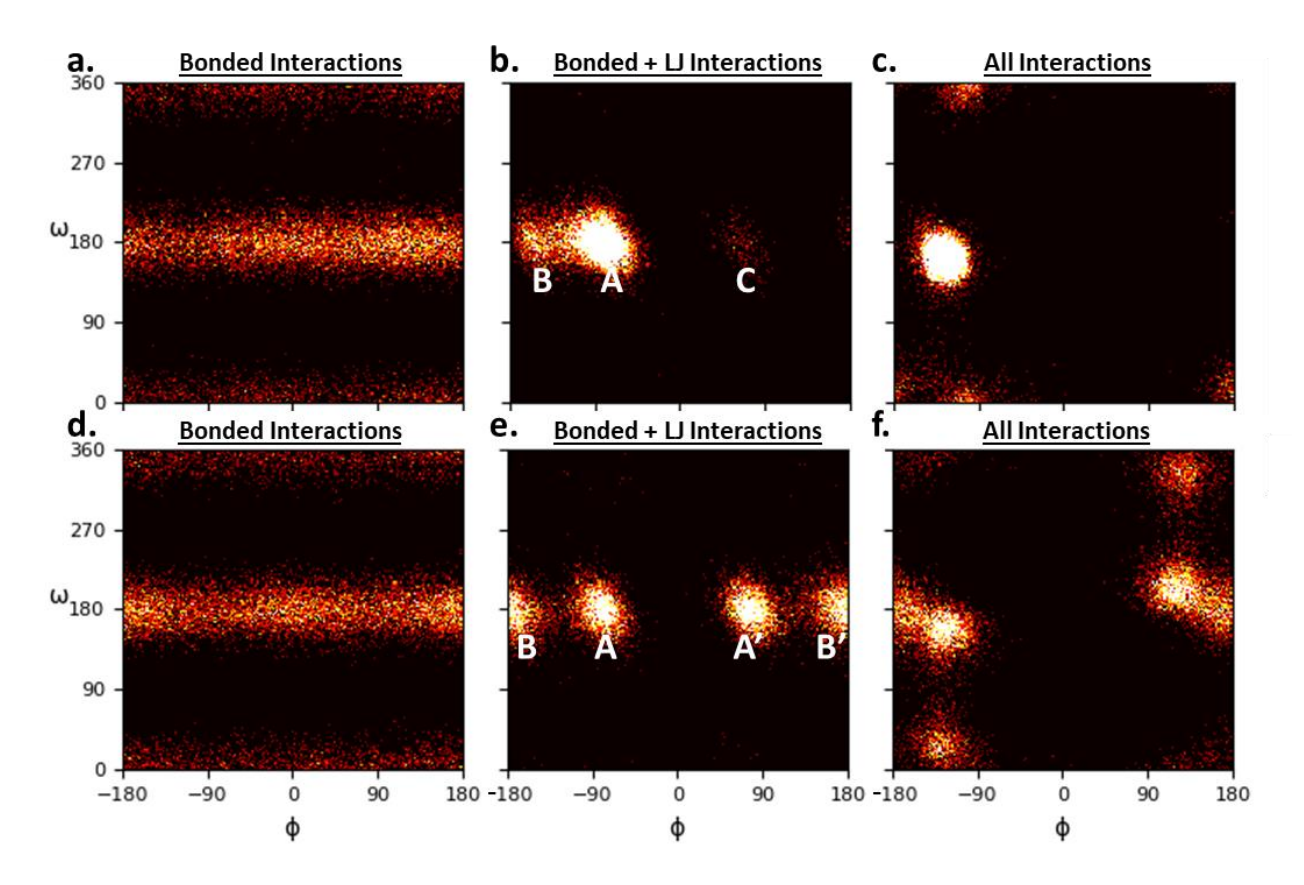


Figure 3. Joint probability distribution for φ - ω torsion angles for Capto MMC (top) and Nuvia cPrime (bottom) in vacuum. (a)/(d) Bonded interactions only. (b)/(e) Bonded interactions + LJ interactions. (c)/(f) All intramolecular interactions (bonded + LJ + electrostatic interactions). Probability is normalized such that the sum over all dimensions goes to 1 and ranges from p = 0 to p = 5e-4 (same scale as Figure 2).

Figure 3b shows the conformational preferences of Capto MMC with bonded and LJ interactions. We find that steric repulsions now eliminate any preference for $\omega = 0^{\circ}/360^{\circ}$, restricting the ligand into conformations near $\omega = 180^{\circ}$. Additionally, preferences for specific values of φ now emerge, as reflected in the conformations A, B, and C, similar to those observed in water. Rotation about the φ angle, while holding ω near 180° , changes the intramolecular distances between several heavy atoms, shifting the balance between LJ attractions and repulsions, stabilizing conformations A, B, and C (see SI).

We observe similar trends in Nuvia cPrime (Figure 3e), where conformations A and B emerge upon adding LJ interactions, accompanied by their counterparts, A' and B'. Because Nuvia cPrime lacks an alkyl thiol tail, steric repulsion in conformation B is reduced, allowing the preference for φ to move toward +/-180°. The reduced steric repulsion also adds symmetry to the central carboxylic acid carbon, as discussed earlier.

Figures 3c and 3f show the conformational preferences of Capto MMC and Nuvia cPrime, respectively, in vacuum with all interactions including bonded and non-bonded interactions. In both molecules, conformational sampling is dominated by electrostatic repulsions between negative partial charges on oxygen atoms of the carboxylic acid and amide groups. This repulsion maximizes the distance between these atoms subject to the constraints of the bonded interactions. These conformations are, however, of limited interest (except perhaps in low dielectric organic solvents or in gas phase), because in water or any high dielectric medium the electrostatic repulsions are screened, as is shown later in the manuscript.

It is interesting to note that for both Capto MMC and Nuvia cPrime we observe that the fluctuations about the mean values of ω and φ for each conformation (*e.g.*, Figures 2, 3b, or 3e) are not radially symmetric, but rather elliptical in shape. As stated previously, the stability of these conformations is governed primarily by the balance of attractive and repulsive LJ interactions. The elliptical shape represents the combinations of φ and ω near the peak that approximately maintain key intramolecular distances, and therefore, the corresponding LJ interactions.

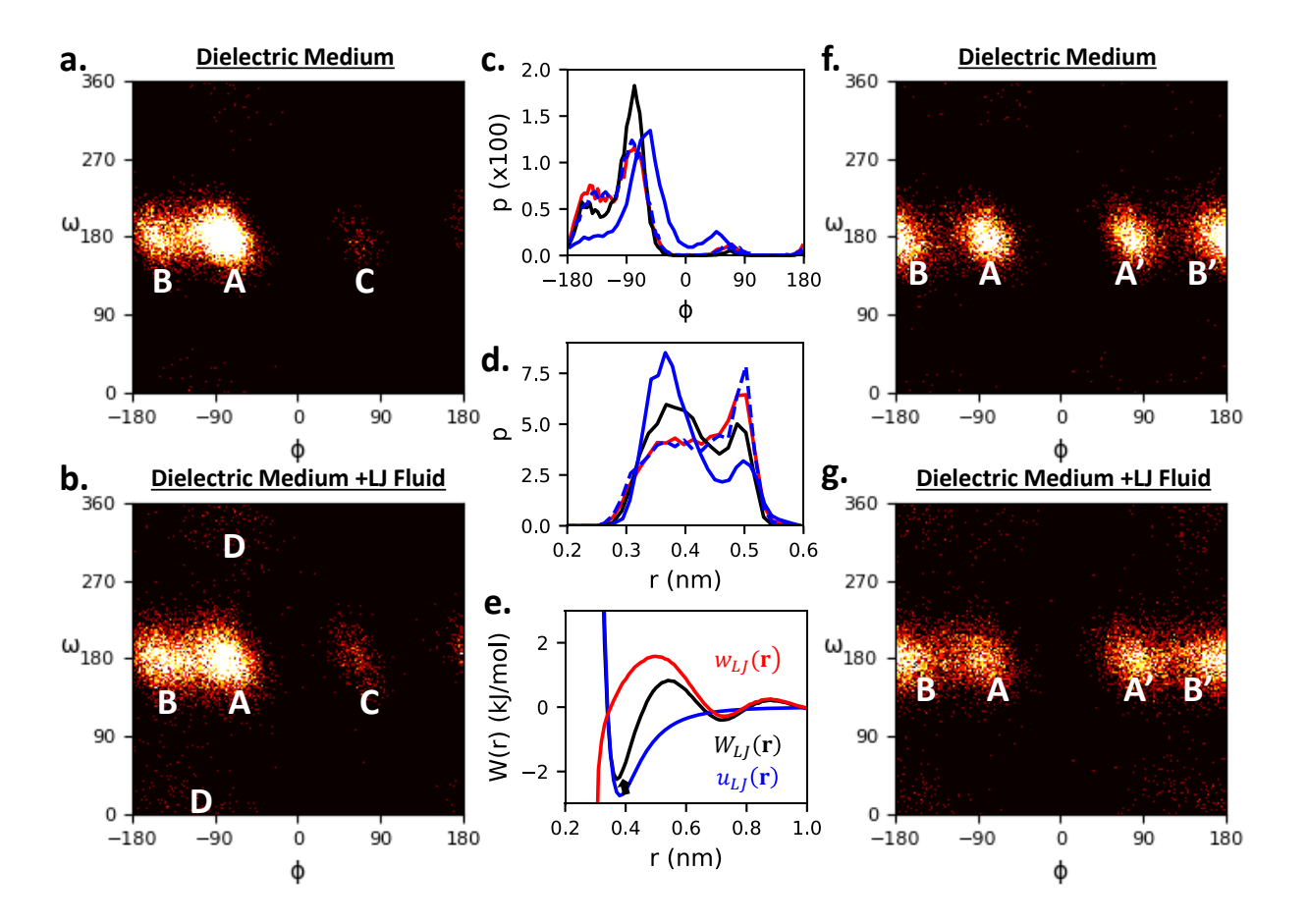


Figure 4. Joint probability distribution for φ - ω torsion angles for Capto MMC in (a) dielectric medium and (b) dielectric medium + LJ liquid. (c) Probability distribution, $p(\varphi)$, in Capto MMC placed in a dielectric medium (black), dielectric medium + LJ liquid (red), and in water (blue). $p(\varphi)$ for an uncharged version of Capto MMC placed in water is also shown (dotted blue line). The peaks in these distributions correspond to conformations A, B, and C (as labelled). (d) Distance distribution between carboxylic acid and amide oxygens for Capto MMC. (e) PMF, W(r) = -kTln[g(r)], for LJ particles in LJ fluid (black) decomposed into the direct interaction (blue) and the solvent contribution (red), where g(r) is the LJ particle-particle radial distribution function. (f) Joint probability distribution for φ - ω torsion angles for Nuvia cPrime in a dielectric medium and (g) dielectric medium + LJ liquid. Probability is normalized such that the sum over all dimensions goes to 1 and ranges from p = 0 to p = 5e-4 (same scale as Figure 2).

The presence of a solvent influences the conformational preferences of a solute in a number of ways. Solvents can provide a dielectric medium that screens electrostatic interactions. The

molecular (or granular) nature of the solvent can lead to local packing and corresponding packing-mediated interactions. Finally, solvents can hydrogen-bond with the solute and/or with themselves, further introducing solvent-mediated interactions. Below we quantify these aspects for the case where the ligand is solvated in an LJ liquid, ethanol, and water in a systematic manner.

Figure 4a shows the conformational equilibria of Capto MMC in a continuum, high dielectric medium ($\epsilon = 78$). As expected, these results are essentially identical to that in vacuum without electrostatic interactions (Figure 3b). Further comparisons between these two cases are presented in SI.

Figure 4b shows the conformational equilibria of Capto MMC in an LJ liquid with additional screening provided by a high dielectric constant ($\varepsilon = 78$). This case is similar to having a ligand without charges that is solvated in a LJ liquid. Introducing an attractive, granular solvent shifts the relative probabilities of the peaks. Specifically, the preference for conformation A decreases and that for B and C increases. One dimensional projection onto the φ axis demonstrates this shift in preference upon the addition of a granular solvent clearly (Figure 4c). In addition, we observe the emergence of conformation D, albeit with a much smaller probability (Figure 4b).

The impact of adding a granular solvent is also visible in the distribution of the distance between the oxygens of carboxylic acid and amide, as shown in Figure 4d. The increase in the probability of conformation B is consistent with increase in the probability of the peak in the distance distribution located near 0.52 nm. Interestingly, the probability of sampling shorter distances between the oxygens (*e.g.*, in between 0.32 to 0.36 nm) is also slightly higher in the LJ solvent. What are the physical origins of these changes?

It is instructive to study a much simpler system, namely two LJ particles in an LJ solvent, and quantify the potential of mean force (PMF) between them. Figure 4e shows the PMF as well as its

resolution into the direct (blue) and solvent-mediated (red) contributions. We notice that upon adding the LJ solvent, the contact configuration destabilizes and moves to slightly shorter distances. A solvent-separated minimum also appears at 0.72 nm. The destabilization of the contact minimum reflects the competition for interactions by the attractive solvent molecules, whereas its inward movement is a result of the so-called osmotic pressure. Thus, the addition of an attractive granular solvent softens the repulsions (*i.e.*, pushes the particles slightly closer), but also decreases the overall stability of those close contacts. These observations are consistent with the conformational shift observed in Figure 4c as well as shifts in distance distributions shown in the inset.

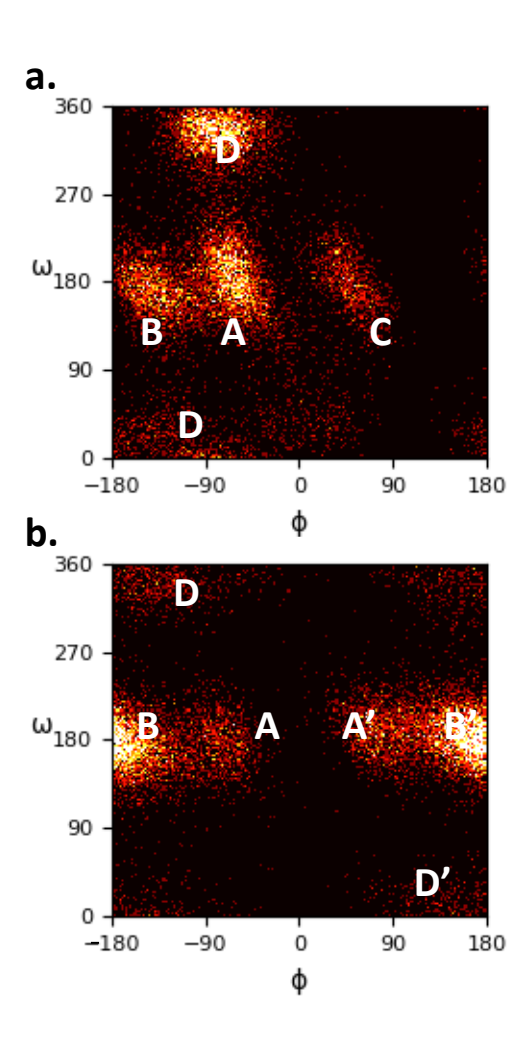


Figure 5. Joint probability distribution for ϕ - ω torsion angles for (a) Capto MMC and (b) Nuvia cPrime in different ethanol simulations. Probability is normalized such that the sum over all dimensions goes to 1 and ranges from p = 0 to p = 5e-4 (same scale as Figure 2).

Figures 4f and 4g show the conformational equilibrium of Nuvia cPrime in a high dielectric medium and in an LJ fluid. The conformational shifts observed for Nuvia cPrime are analogous to those observed for Capto MMC, with the exception that reduced steric repulsion allows for additional symmetry.

Figures 5a and 5b show the conformational equilibria for Capto MMC and Nuvia cPrime, respectively, in pure ethanol. Like water, ethanol is a hydrogen-bonding liquid, but unlike water, it is not capable of forming bi-directional hydrogen-bonded chains due to the presence of the ethyl group. Conformational equilibria in ethanol are similar to those in water, although they differ slightly in the locations of maxima as well as their precise size and shape (see SI). Importantly, in both ethanol and water there is significant population of conformation D. As was discussed earlier, solvent-mediated interactions must contribute to overcome the unfavorable intramolecular torsion angle potential on ω . The significant population of D in water and ethanol suggests that hydrogen-bonding interactions with the solvent are important contributors to the stability of these conformations. Interestingly, for Nuvia cPrime, in addition to the emergence of the conformation D, we find that conformation B is preferred over A.

The importance of solute-solvent hydrogen bonding in stabilizing conformation D is illustrated in Figures 6a-d. Figure 6a shows the conformational preferences of a version of Capto MMC without electrostatic charges solvated in water. In the absence of solute-water hydrogen bonding, conformation D appears with a low probability. Interestingly, these conformational equilibria are nearly identical to those of the charged ligand in an LJ fluid with $\varepsilon = 78$ (Figure 4b), where solvent-

solute hydrogen bonding is also not possible. As might be expected, one dimensional projections of the conformational equilibrium on φ or ω axes (Figures 4c and 6b, respectively) and the distribution of the distance between oxygen atoms is also nearly identical for the above two solute-solvent combinations. Comparisons between these two systems using a Kolmogorov-Smirnov test can be found Supporting Information.

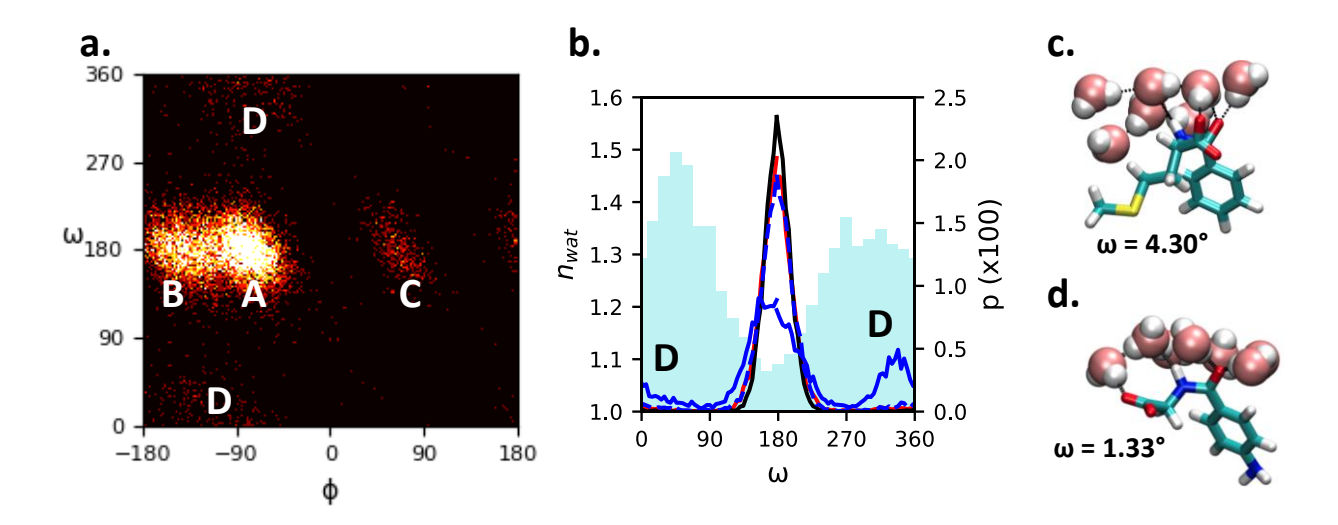


Figure 6. (a) Joint probability, $p(\varphi, \omega)$, for Capto MMC without charges in water using the same convention as Figure 2. (b) $p(\omega)$ in Capto MMC in the various media is also shown (with same convention as Figures 4a and 4c). The average number of water molecules in the hydration shell (3Å) of the amide hydrogen as a function of ω is shown in the background (cyan bars). (c) and (d) Snapshots of Capto MMC and Nuvia cPrime (licorice) hydrogen bonding with neighboring water molecules (spacefill). (Color scheme: hydrogen, white; oxygen, red; carbon, cyan; nitrogen, blue; and sulfur, yellow).

The background in Figure 6b shows the average number of water molecules in the hydration shell of the amide hydrogen atom as a function of ω (cyan). It is evident that as ω changes from its stable value of 180° (trans configuration) toward 0°/360° (conformation D) the amide hydrogen is better hydrated with the addition of about 0.4 water molecules to its hydration shell on average. Snapshots of D conformations obtained from molecular simulations of Capto MMC and Nuvia

cPrime (Figures 6c and 6d) show that *cis* conformations enable hydrogen bonding of amide hydrogen with the hydration water and also enable the amide hydrogen and oxygen to interact through chains of either one or two hydrogen-bonded water molecules.

To summarize: the conformational equilibria of an uncharged ligand in water are similar to that of a charged ligand in high dielectric LJ solvent, with a low probability for conformation D. In contrast, the conformational equilibria of Capto MMC and Nuvia cPrime are similar in water and in ethanol, with a higher probability for conformation D. The amide group displays enhanced hydration and hydrogen bonding with water in *cis* (D-like) conformations relative to the trans conformations (A, B, and C). Collectively, these observations highlight the importance of solute-solvent hydrogen bonding interactions in stabilizing conformation D.

3.3 Conformation Upon Binding to a Protein: The Role of Direct Ligand-Protein Interactions

In a typical commercial application, Capto MMC and Nuvia cPrime are immobilized on chromatography beads, which are packed in a column and used to separate complex mixtures of proteins⁵³. Synergistic interactions between the multiple modes of interaction present in these ligands enable separation of proteins differing by as little as a single mutation^{24,54–56}. The conformational equilibria of ligands attached to resins depend on various factors, including the nature of the attachment, the density of ligands on the surface, and other details. Binding of a protein to the ligand-covered surface may cause additional changes in the conformational equilibrium of a ligand.

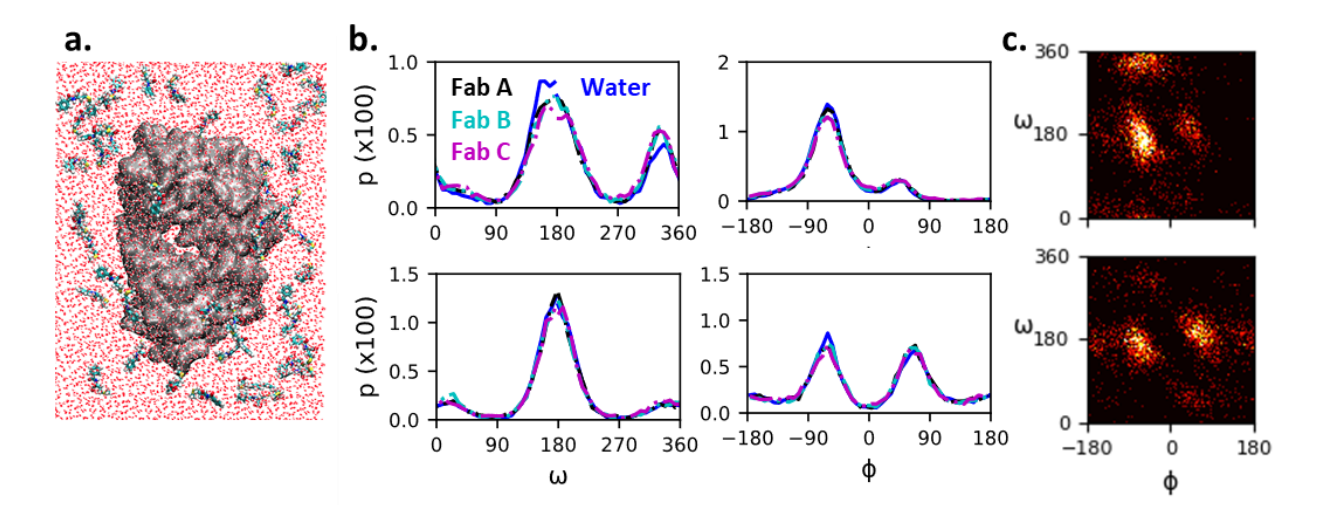


Figure 7. (a) A snapshot from MD simulations of a protein (Fab A, shown with grey surface representation) in an aqueous solution with Capto MMC ligands. (water – wireframe, ligand – licorice with same color scheme as in previous figures). (b) Distributions, $P(\omega)$ and $P(\phi)$, for Capto MMC (top) and Nuvia cPrime (bottom) in water and bound to proteins. (c) $P(\phi,\omega)$ for Capto MMC (top) and Nuvia cPrime (bottom) while bound to Fab A (scale same as in Figure 2).

As a step towards understanding ligand conformational equilibria in chromatographic systems, we examine ligand conformational changes upon binding to protein surfaces. As described in the methods section, we selected three different proteins, Fab A, Fab B, and Fab C, which are fragments of three different antibodies representative of typical protein therapeutics. These proteins have different distributions of hydrophobic, polar, and charged regions on the surface as described in a previous paper from our group⁵¹. We placed each protein in the center of a box surrounded by ligands in free solution as shown in Figure 7a and performed 200ns long simulations, saving frames every 1ps. We selected frames every 50ps to perform conformational analysis of bound ligands, thus using over 100,000 bound ligand conformations per simulation to analyze ligand behavior.

Figures 7b and 7c show that conformational preferences of Capto MMC and Nuvia cPrime bound to the surfaces of Fab A, Fab B, and Fab C are nearly identical to those observed previously in water. As stated above, the surfaces of the three proteins represent significant diversity of patterns of hydrophobic, polar, and charged groups. Additionally, on a given protein, a ligand binds at many different locations, thus sampling a diversity of chemical and topographical contexts (shown in Supporting Information). Despite this diversity, the overall conformational preferences of ligands are found to be similar to that in water (Kolmogorov-Smirnov statistics are shown in Supporting Information).

We expect conformations A, B and C ($\omega \approx 180^\circ$) to be relatively unaffected upon binding as they are stabilized primarily by intramolecular interactions within the ligand. Interestingly, conformation D ($\omega \approx 0^\circ/360^\circ$), which is stabilized by hydrogen bonding with solvent, also remains unaffected upon binding to the protein. This leads to several questions: what is the extent of ligand dehydration upon binding to the protein? Are the key water molecules that stabilize conformation D retained in the bound configurations? Do protein atoms hydrogen bond with ligand atoms, essentially replacing the key hydrogen-bonding water molecules?

Figure 8 shows the distributions of the total numbers of water molecules in the hydration shell of Capto MMC (top) and Nuvia cPrime (bottom) in free solution and when bound to the protein Fab A. The hydration shell fluctuations are approximately Gaussian for Capto MMC and Nuvia cPrime, as is expected. Upon binding to the protein surface, the average number of hydration shell water molecules decreases from about 117 to 84 for Capto MMC (~30% decrease) and from about 103 to 79 for Nuvia cPrime (~20% decrease), indicating a partial dehydration of the bound ligand. The distribution of the number of water molecules in the hydration shell of a bound ligand remains approximately Gaussian for both ligands. For ligands (or drug molecules) that bind strongly in a

specific pocket, one might expect almost complete dehydration of the ligand. The partial dewetting observed here is consistent with the fact that multimodal ligands bind to proteins with moderate affinity (Kd $\sim 1~\mu M$) at multiple locations on the surface^{32,57}.

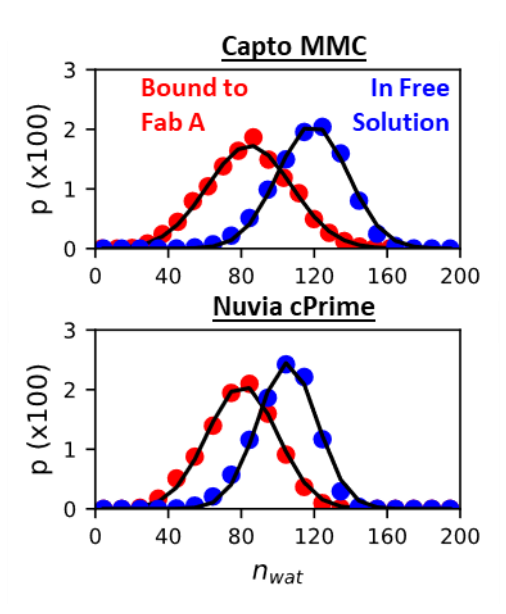


Figure 8. Distribution of the number of water molecules (dots) in the hydration shell of Capto MMC (top) and Nuvia cPrime (bottom) and Gaussian fits of those distributions (black line). Water oxygens within 3Å of heavy atoms of ligands are counted as being in the hydration shell.

Figures 9a-f shows distributions of numbers of water molecules coordinating the hydrogen bonding sites on both ligands in water and in the bound states on proteins. These sites are also dehydrated in the bound state, but the extent of dehydration is far less than that of the overall ligand. A few key differences can be noted for the hydration of hydrogen bonding sites on the ligand. The distributions are wider in the bound state, and the probability of observing zero water molecules in the hydration shell is higher. The insets of Figures 9b and 9e show that the number of hydration shell water molecules depends on ω such that hydrogen bonding sites are more dehydrated in the conformations A, B, and C ($\omega = 180^{\circ}$) and slightly more hydrated in conformation D (ω near 0° and 360°).

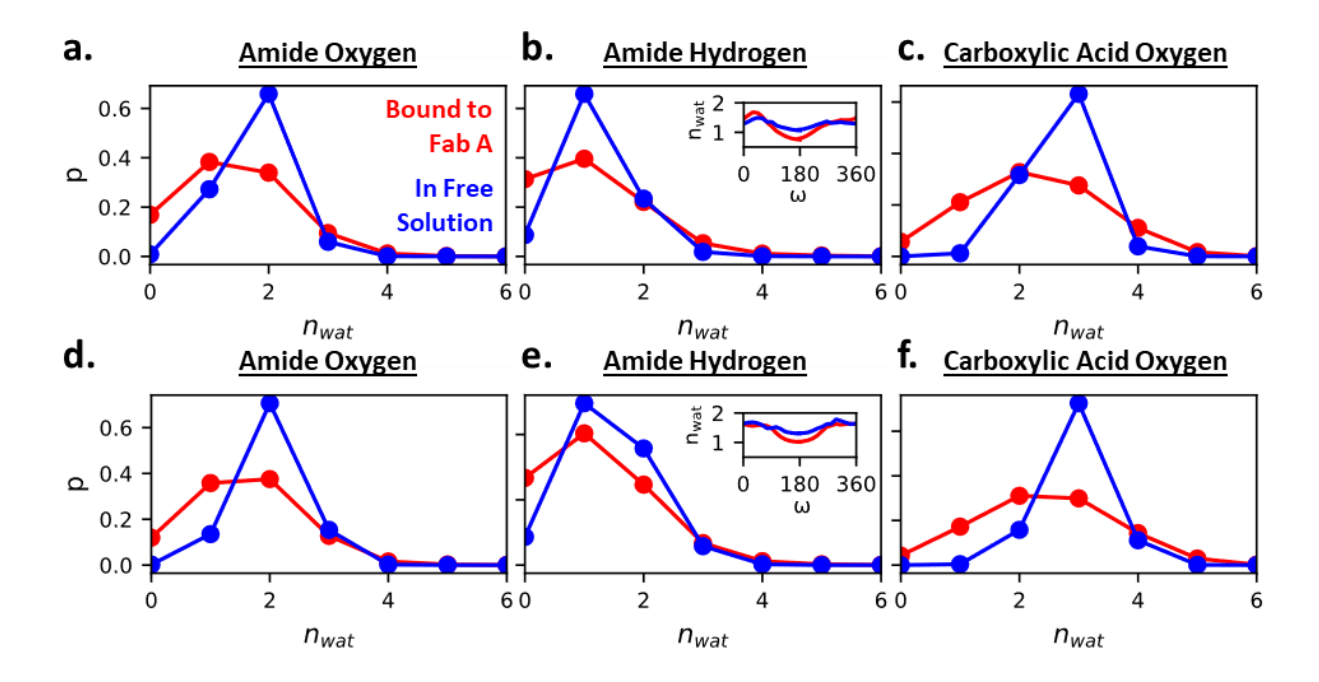


Figure 9. Distribution of the number of water molecules in the hydration shell (3Å) of the three hydrogen bonding sites on Capto MMC (a-c) and Nuvia cPrime (d-f). Inset: Average number of water molecules in the hydration shell of the amide hydrogen as a function of ω .

These results suggest that, depending on the local context, the hydrogen bonding sites on the ligand might either maintain their hydrogen bonding water partners, or lose them in such a way that specific protein atoms serve as hydrogen bonding partners. For example, Figure 10a shows a snapshot of Capto MMC bound to a site on the surface of Fab A, with water molecules hidden for clarity. In this instance, the ligand is partially dehydrated, burying the amide group and parts of the phenyl ring and alkyl thiol group. Figure 10b illustrates the interactions occurring in Figure 10a mapped onto a two-dimensional graph. We see that for this bound pose, the amide oxygen and hydrogen are hydrogen bonded to atoms within the protein, while the carboxylic acid oxygens are hydrogen bonded to nearby water molecules, which are in turn hydrogen bonded to one another.

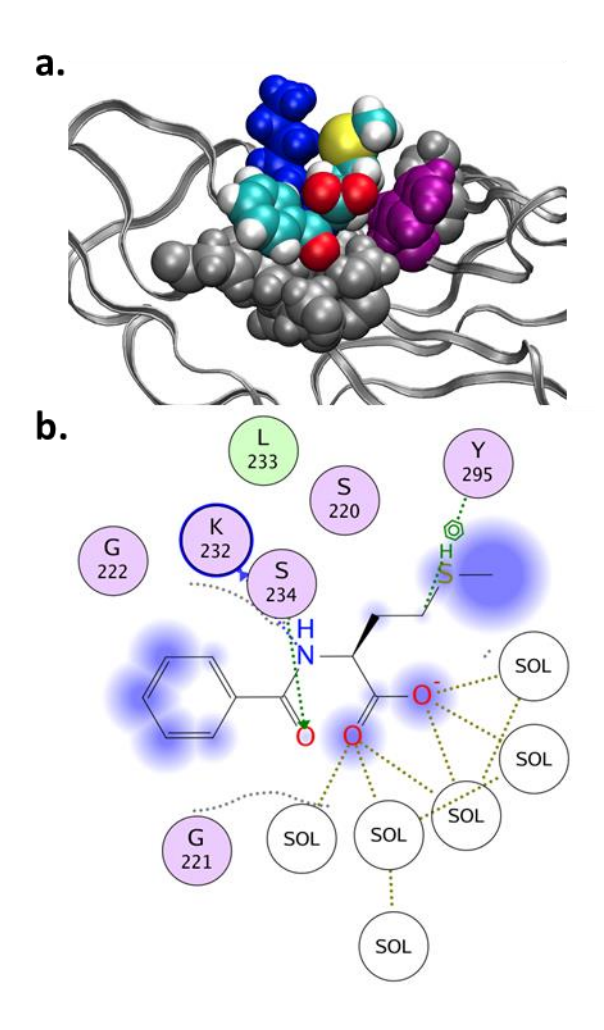


Figure 10. (a) Representative snapshot showing Capto MMC bound to Fab A. Protein is shown using ribbon structure, the ligand and the residues within 4Å are shown in spacefill (polar residues, grey; positively charged residues, blue; aromatic residues, purple; carbon, cyan; hydrogen, white; oxygen, red; sulfur, yellow; nitrogen, blue), water molecules are hidden for clarity. **(b)** 2D schematic generated using MOE⁵⁸ (Chemical Computing Group) showing hydrogen bonding interactions between protein residues, ligand atoms, and water molecules (labelled SOL). Polar residues are shown in purple and hydrophobic residues are shown in green. Solvent-exposed regions of the ligand are highlighted in blue. Sizes and distances are not shown to scale.

4. Conclusions

We reported results from molecular dynamics simulations focused on the conformational equilibria of two ligands important in multimodal chromatography, Capto MMC and Nuvia cPrime, in water as well as in the vicinity of proteins. Both ligands are small and have limited flexibility such that much of the important ligand conformational space is characterized by mapping the distributions of two internal dihedral angles, ω and φ . Studying the ligands in vacuum and in a series of solvents – an LJ liquid, ethanol, and water – revealed the relative importance of intramolecular and solvent-mediated interactions, including hydrogen bonding with solvent molecules. We found that in the φ - ω space, Capto MMC displays preference for four distinct conformations, referred to as A, B, and C, which are stabilized by intramolecular interactions, and conformation D, which is stabilized by solvent-mediated (hydrogen bonding) interactions. The behavior of Nuvia cPrime is similar to that of Capto MMC, except that because of additional symmetry present in the molecule, it samples only three distinct conformations A, B, and D and their symmetric counterparts A', B', and D'. Interestingly, for both ligands, conformational preferences are effectively unchanged when the ligands are bound to proteins.

Comparisons of ligand conformational preferences in vacuum and in various granular solvents bring out interesting features of the effects of solvent granularity and solute-solvent interactions, in particular hydrogen-bonding interactions. For example, a granular solvent with attractive interactions (*e.g.*, an LJ liquid) 'flattens out' the conformational landscape observed in vacuum. Thus, peaks in probability distributions in vacuum, which are stabilized by intramolecular interactions, are broadened as the solvent competes with intramolecular interactions. Solvent-mediated interactions between sites push site-site contacts closer (which can be understood in terms of solvent osmotic pressure), while simultaneously reducing the stability of contact configurations. The presence of a solvent can also introduce solvent-separated minima at a larger

distance, at which one solvent molecule can sit comfortably between two solute sites, solvating both of them.

We showed that the introduction of a hydrogen bonding solvent leads to the stabilization of conformation D, for which the amide bond is in near-cis conformation. Non-proline cis configurations of peptide bonds have been found in enzymes and other proteins often near active sites or binding sites, which are also stabilized by hydrogen bonding interactions^{59,60}.

Finally, we showed that the ligand conformational preferences remain essentially unchanged regardless of where on each protein's surface a ligand is bound. We showed that although the overall ligand is partially dehydrated (by about 20-30%) when bound to a protein (see Figure 7), hydrogen bonding sites on the ligand have a lower probability of dehydration (see Figure 8). In instances, where these sites dehydrate, we showed that protein atoms replace water as a hydrogen bonding partner, thus maintaining ligand conformation via a combination of interactions with retained water molecules and protein hydrogen-bonding sites.

It is instructive to compare protein-ligand binding in multimodal chromatography to a similar application, protein-drug binding. Drugs are typically small molecules that bind to specific sites on the protein surface through multiple modes of interaction with high affinity $(K_d \sim 1 \text{nM})^{61}$. Multimodal ligands are similar in that they are small molecules that bind through multiple modes of interaction but differ in that they bind weakly $(K_d \sim 1 \mu \text{M})^{57}$ and often to multiple regions on the protein surface³². This is because a good multimodal resin must be able to (i) solve a wide range of protein separation challenges, regardless of protein structure and sequence, and (ii) allow elution of the protein of interest (in addition to binding it). These considerations make multimodal ligand design related to, yet distinct from drug design.

In this work, we have characterized ligand conformational equilibria in free solution and bound to proteins. In chromatography, multimodal ligands are tethered to the surface of a porous bead. We anticipate that the introduction of a surface will impact solvent structuring in the vicinity of the ligand, thus changing ligand conformational preferences. We also expect that differences in ligand flexibility near the point of attachment will impact the space that ligands are able to sample in the vicinity of the surface. Our results provide an excellent reference for studies of those inhomogeneous systems, which is the subject of ongoing investigation in our group. Additionally, in chromatography, solvent conditions including pH and salt are typically used to reduce protein-ligand interactions and drive elution. In the future, we plan to extend our work to explore these solvent effects on ligand conformation in free solution and in the context of a surface.

Supporting Information. Ligand parameterization details (charges assigned by RESP and Lennard Jones parameters), detailed evaluation of the relationship between intramolecular interactions and conformational preferences observed in a vacuum and a high dielectric continuum, torsion angles replotted in one dimension (as opposed to two dimensional plots shown in text) to facilitate additional comparison, and protein-ligand binding hotspots on Fab A, Fab B, and Fab C.

5. Acknowledgements

This material is based upon work partially supported by the National Science Foundation under Grant No. (CBET 1704745) as well as the ASC Graduate Fellowship Program from LLNL. The authors would also like to acknowledge helpful discussions with Dr. David Roush from Merck & Co., Inc. and Dr. Mark Snyder from Bio-Rad. Work at the Lawrence Livermore National

Laboratory (LLNL) was performed under the auspices of the U.S. Department of Energy by Lawrence Livermore National Laboratory under Contract DE-AC52-07NA27344.

6. References

- (1) Israelachvili, J. N. Intermolecular and Surface Forces, 3. ed.; Elsevier, Acad. Press: Amsterdam, 2011.
- (2) Tanford, C. Hydrophobic Effect: Formation of Micelles and Biological Membranes, 1st ed.; John Wiley & Sons Inc, 1973.
- (3) Dill, K. A.; Bromberg, S. Molecular Driving Forces: Statistical Thermodynamics in Biology, Chemistry, Physics, and Nanoscience, 2nd ed.; Garland Science, 2013.
- (4) Pangali, C.; Rao, M.; Berne, B. J. On a Novel Monte Carlo Scheme for Simulating Water and Aqueous Solutions. Chem. Phys. Lett. 1978, 55 (3), 5.
- (5) Ashbaugh, H. S.; Weiss, K.; Williams, S. M.; Meng, B.; Surampudi, L. N. Temperature and Pressure Dependence of Methane Correlations and Osmotic Second Virial Coefficients in Water. J. Phys. Chem. B 2015, 119 (20), 6280–6294.
- (6) Garde, S.; Hummer, G.; Paulaitis, M. E. Hydrophobic Interactions: Conformational Equilibria and the Association of Non-Polar Molecules in Water. Faraday Discuss. 1996, 103, 125.
- (7) Day, R.; Paschek, D.; Garcia, A. E. Microsecond Simulations of the Folding/Unfolding
 Thermodynamics of the Trp-Cage Miniprotein. Proteins Struct. Funct. Bioinforma. 2010, NA-NA.
- (8) Hummer, G.; García, A. E.; Garde, S. Conformational Diffusion and Helix Formation Kinetics. Phys. Rev. Lett. 2000, 85 (12), 2637–2640.
- (9) Drozdov, A. N.; Grossfield, A.; Pappu, R. V. Role of Solvent in Determining Conformational Preferences of Alanine Dipeptide in Water. J. Am. Chem. Soc. 2004, 126 (8), 2574–2581.
- (10) Ferguson, A. L.; Debenedetti, P. G.; Panagiotopoulos, A. Z. Solubility and Molecular Conformations of n -Alkane Chains in Water. J. Phys. Chem. B 2009, 113 (18), 6405–6414.
- (11) Athawale, M. V.; Goel, G.; Ghosh, T.; Truskett, T. M.; Garde, S. Effects of Lengthscales and Attractions on the Collapse of Hydrophobic Polymers in Water. Proc. Natl. Acad. Sci. 2007, 104 (3), 733–738.
- (12) Underwood, R.; Tomlinson-Phillips, J.; Ben-Amotz, D. Are Long-Chain Alkanes Hydrophilic? J. Phys. Chem. B 2010, 114 (26), 8646–8651.
- (13) Selig, O.; Cunha, A. V.; van Eldijk, M. B.; van Hest, J. C. M.; Jansen, T. L. C.; Bakker, H. J.; Rezus, Y. L. A. Temperature-Induced Collapse of Elastin-like Peptides Studied by 2DIR Spectroscopy. J. Phys. Chem. B 2018, 122 (34), 8243–8254.
- (14) Jamadagni, S. N.; Bosoy, C.; Garde, S. Designing Heteropolymers To Fold into Unique Structures via Water-Mediated Interactions. J. Phys. Chem. B 2010, 114 (42), 13282–13288.
- (15) Blatt, H. D.; Smith, P. E.; Pettitt, B. M. Protonation Effects on the Equilibrium and Dynamical Properties of the Alanine Tetrapeptide. J. Phys. Chem. B 1997, 101 (38), 7628–7634.

- (16) Mirkin, N. G.; Krimm, S. Conformation Dependence of the C α D α Stretch Mode in Peptides. II. Explicitly Hydrated Alanine Peptide Structures. Biopolymers 2009, 91 (9), 791–800.
- (17) Mirkin, N. G.; Krimm, S. Water Interaction Differences Determine the Relative Energetic Stability of the Polyproline II Conformation of the Alanine Dipeptide in Aqueous Environments. Biopolymers 2012, 97 (10), 789–794.
- (18) Busch, S.; Bruce, C. D.; Redfield, C.; Lorenz, C. D.; McLain, S. E. Water Mediation Is Essential to Nucleation of β-Turn Formation in Peptide Folding Motifs. *Angew. Chem. Int. Ed.* **2013**, *52* (49), 13091–13095.
- (19) Meral, D.; Toal, S.; Schweitzer-Stenner, R.; Urbanc, B. Water-Centered Interpretation of Intrinsic PPII Propensities of Amino Acid Residues: *In Vitro* -Driven Molecular Dynamics Study. *J. Phys. Chem. B* **2015**, *119* (42), 13237–13251.
- (20) Jong, K.; Hassanali, A. A. A Data Science Approach to Understanding Water Networks Around Biomolecules: The Case of Tri-Alanine in Liquid Water. *J. Phys. Chem. B* **2018**, *122* (32), 7895–7906.
- (21) Jamadagni, S. N.; Godawat, R.; Garde, S. Hydrophobicity of Proteins and Interfaces: Insights from Density Fluctuations. *Annu. Rev. Chem. Biomol. Eng.* **2011**, *2* (1), 147–171.
- (22) Jamadagni, S. N.; Godawat, R.; Dordick, J. S.; Garde, S. How Interfaces Affect Hydrophobically Driven Polymer Folding [†]. *J. Phys. Chem. B* **2009**, *113* (13), 4093–4101.
- (23) Murina, E. L.; Fernández-Prini, R.; Pastorino, C. Molecular Conformation of Linear Alkane Molecules: From Gas Phase to Bulk Water through the Interface. *J. Chem. Phys.* **2017**, *147* (6),
- (24) Chung, W. K.; Hou, Y.; Holstein, M.; Freed, A.; Makhatadze, G. I.; Cramer, S. M. Investigation of Protein Binding Affinity in Multimodal Chromatographic Systems Using a Homologous Protein Library. *J. Chromatogr. A* **2010**, *1217* (2), 191–198.
- (25) Gagnon, P.; Cheung, C.-W.; Lepin, E. J.; Wu, A. M.; Sherman, M. A.; Yazaki, P. J. Minibodies and Multimodal Chromatography Methods: **2011**, 21.
- (26) Kaleas, K. A.; Schmelzer, C. H.; Pizarro, S. A. Industrial Case Study: Evaluation of a Mixed-Mode Resin for Selective Capture of a Human Growth Factor Recombinantly Expressed in E. Coli. *J. Chromatogr. A* **2010**, *1217* (2), 235–242.
- (27) Shukla, A. A.; Hubbard, B.; Tressel, T.; Guhan, S.; Low, D. Downstream Processing of Monoclonal Antibodies—Application of Platform Approaches. *J. Chromatogr. B* **2007**, *848* (1), 28–39.
- (28) Sejergaard, L.; Karkov, H. S.; Krarup, J. K.; Hagel, A. B. B.; Cramer, S. M. Model-Based Process Development for the Purification of a Modified Human Growth Hormone Using Multimodal Chromatography. *Biotechnol. Prog.* **2014**, *30* (5), 1057–1064.
- (29) Chmielowski, R. A.; Meissner, S.; Roush, D.; Linden, T. O.; Glowacki, E.; Konietzko, J.; Nti-Gyabaah, J. Resolution of Heterogeneous Charged Antibody Aggregates via Multimodal Chromatography: A Comparison to Conventional Approaches. *Biotechnol. Prog.* **2014**, *30* (3), 636–645.
- (30) Zhao, G.; Dong, X.-Y.; Sun, Y. Ligands for Mixed-Mode Protein Chromatography: Principles, Characteristics and Design. *J. Biotechnol.* **2009**, *144* (1), 3–11.
- (31) Cramer, S. M.; Holstein, M. A. Downstream Bioprocessing: Recent Advances and Future Promise. *Curr. Opin. Chem. Eng.* **2011**, *1* (1), 27–37.
- (32) Parimal, S.; Garde, S.; Cramer, S. M. Interactions of Multimodal Ligands with Proteins: Insights into Selectivity Using Molecular Dynamics Simulations. *Langmuir* **2015**, *31* (27), 7512–7523.
- (33) Banerjee, S.; Parimal, S.; Cramer, S. M. A Molecular Modeling Based Method to Predict Elution Behavior and Binding Patches of Proteins in Multimodal Chromatography. *J. Chromatogr. A* **2017**, 1511, 45–58.
- (34) Wang, J.; Wolf, R. M.; Caldwell, J. W.; Kollman, P. A.; Case, D. A. Development and Testing of a General Amber Force Field. *J. Comput. Chem.* **2004**, *25* (9), 1157–1174.

- (35) Bayly, C. I.; Cieplak, P.; Cornell, W.; Kollman, P. A. A Well-Behaved Electrostatic Potential Based Method Using Charge Restraints for Deriving Atomic Charges: The RESP Model. J. Phys. Chem. 1993, 97 (40), 10269–10280.
- (36) Wang, J.; Cieplak, P.; Kollman, P. A. How Well Does a Restrained Electrostatic Potential (RESP) Model Perform in Calculating Conformational Energies of Organic and Biological Molecules? *J. Comput. Chem.* **2000**, *21* (12), 1049–1074.
- (37) Wang, J.; Wang, W.; Kollman, P. A.; Case, D. A. Antechamber, An Accessory Software Package For Molecular Mechanical Calculations. *J. Am. Chem. Soc.* **2001**, *222*, 41.
- (38) Sousa da Silva, A. W.; Vranken, W. F. ACPYPE AnteChamber PYthon Parser Interface. *BMC Res. Notes* **2012**, *5* (1), 367.
- (39) Berendsen, H. J. C.; van der Spoel, D.; van Drunen, R. GROMACS: A Message-Passing Parallel Molecular Dynamics Implementation. *Comput. Phys. Commun.* **1995**, *91* (1–3), 43–56.
- (40) Hess, B.; Kutzner, C.; van der Spoel, D.; Lindahl, E. GROMACS 4: Algorithms for Highly Efficient, Load-Balanced, and Scalable Molecular Simulation. *J. Chem. Theory Comput.* **2008**, *4* (3), 435–447.
- (41) Pronk, S.; Páll, S.; Schulz, R.; Larsson, P.; Bjelkmar, P.; Apostolov, R.; Shirts, M. R.; Smith, J. C.; Kasson, P. M.; van der Spoel, D.; et al. GROMACS 4.5: A High-Throughput and Highly Parallel Open Source Molecular Simulation Toolkit. *Bioinformatics* **2013**, *29* (7), 845–854.
- (42) Patriksson, A.; van der Spoel, D. A Temperature Predictor for Parallel Tempering Simulations. *Phys. Chem. Chem. Phys.* **2008**, *10* (15), 2073.
- (43) Evans, D.; Holian, B. The Nose-Hoover Thermostat. J. Chem. Phys. 1985, 83 (4069).
- (44) Braun, E.; Moosavi, S. M.; Smit, B. Anomalous Effects of Velocity Rescaling Algorithms: The Flying Ice Cube Effect Revisited. *J. Chem. Theory Comput.* **2018**, *14* (10), 5262–5272.
- (45) Tironi, I. G.; Sperb, R.; Smith, P. E.; van Gunsteren, W. F. A Generalized Reaction Field Method for Molecular Dynamics Simulations. *J. Chem. Phys.* **1995**, *102* (5451).
- (46) Parrinello, M.; Rahman, A. Crystal Structure and Pair Potentials: A Molecular-Dynamics Study. *Phys. Rev. Lett.* **1980**, *45* (14), 1196–1199.
- (47) Darden, T.; York, D.; Pedersen, L. Particle Mesh Ewald An N·log(N) Method for Ewald Sums in Large Systems. **1993**, *98* (10089).
- (48) Frisch, M.J.E.A., Trucks, G.W., Schlegel, H.B., Scuseria, G.E., Robb, M.A., Cheeseman, J.R., Scalmani, G., Barone, V., Mennucci, B., Petersson, G. and Nakatsuji,. Gaussian 09, Revision a. 02, Gaussian. *Inc Wallingford CT 200* **2009**.
- (49) Jorgensen, W. L. Quantum and Statistical Mechanical Studies of Liquids. 10. Transferable Intermolecular Potential Functions for Water, Alcohols, and Ethers. Application to Liquid Water. *J. Am. Chem. Soc.* **1981**, *103* (2), 335–340.
- (50) Huggins, D. J. Correlations in Liquid Water for the TIP3P-Ewald, TIP4P-2005, TIP5P-Ewald, and SWM4-NDP Models. *J. Chem. Phys.* **2012**, *136* (6), 064518.
- (51) Robinson, J.; Roush, D.; Cramer, S. Domain Contributions to Antibody Retention in Multimodal Chromatography Systems. *J. Chromatogr. A* **2018**.
- (52) Cheatham, T.; Cieplak, P.; Kollman, P. A. A Modified Version of the Cornell et Al. Force Field with Improved Sugar Pucker Phases and Helical Repeat. *J. Biomol. Struct. Dyn.* **1999**, *16* (4), 845–862.
- (53) Woo, J.; Parimal, S.; Brown, M. R.; Heden, R.; Cramer, S. M. The Effect of Geometrical Presentation of Multimodal Cation-Exchange Ligands on Selective Recognition of Hydrophobic Regions on Protein Surfaces. *J. Chromatogr. A* **2015**, *1412*, 33–42.
- (54) Karkov, H. S.; Krogh, B. O.; Woo, J.; Parimal, S.; Ahmadian, H.; Cramer, S. M. Investigation of Protein Selectivity in Multimodal Chromatography Using in Silico Designed Fab Fragment Variants. *Biotechnol. Bioeng.* 2015, 112 (11), 2305–2315.

- (55) Holstein, M. A.; Chung, W. K.; Parimal, S.; Freed, A. S.; Barquera, B.; McCallum, S. A.; Cramer, S. M. Probing Multimodal Ligand Binding Regions on Ubiquitin Using Nuclear Magnetic Resonance, Chromatography, and Molecular Dynamics Simulations. J. Chromatogr. A 2012, 1229, 113–120.
- (56) Chung, W. K.; Freed, A. S.; Holstein, M. A.; McCallum, S. A.; Cramer, S. M. Evaluation of Protein Adsorption and Preferred Binding Regions in Multimodal Chromatography Using NMR. *Proc. Natl. Acad. Sci.* **2010**, *107* (39), 16811–16816.
- (57) Zhu, M.; Carta, G. Protein Adsorption Equilibrium and Kinetics in Multimodal Cation Exchange Resins. *Adsorption* **2016**, *22* (2), 165–179.
- (58) Chemical Computing Group. *Molecular Operating Environment (MOE)*.
- (59) Fischer, G. Chemical Aspects of Peptide Bond Isomerisation. *Chem. Soc. Rev.* **2000**, *29* (2), 119–127.
- (60) Fesus, L.; Piacentini, M. Transglutaminase 2: An Enigmatic Enzyme with Diverse Functions. *Trends Biochem. Sci.* **2002**, *27* (10), 534–539.
- (61) Copeland, R. A. The Drug–Target Residence Time Model: A 10-Year Retrospective. *Nat. Rev. Drug Discov.* **2016**, *15* (2), 87–95.

TOC Graphic

